Forward and Reverse Combustion Linking in Underground Coal Gasification

M.S. Blinderman [1], D.N. Saulov [*,2], A.Y. Klimenko [2]

Abstract

In the present study, two techniques used for wells linking in Underground Coal Gasification (UCG), namely, Reverse Combustion Linking (RCL) and Forward Combustion Linking (FCL) are compared. Linking time in FCL is estimated using two-dimensional model and assuming stability of the combustion front. Effects of instabilities during FCL are discussed.

Key words: Underground Coal Gasification, Reverse Combustion Linking, Forward Combustion Linking

1. Introduction

Underground Coal Gasification (UCG) is a process of conversion of coal in coal seams into synthesis gas (syngas) using injection and production wells drilled from the surface. The key step in the development of the underground reactor is establishing a link between the injection and production wells which allows production of syngas at commercially significant flow rates. As described, for example, by Skafa [1], several techniques can be used for linking the wells, including the Reverse Combustion Linking (RCL) and the Forward Combustion Linking (FCL). The RCL is a method of linking which includes injection of an oxidant into one well and ignition of coal in the other so that combustion propagates towards the source of oxidant as shown in Fig. 1(a). In the course of the the FCL coal is ignited in the injection well, and the fire propagates toward the production well as shown in Fig. 1(b).

Flow of oxidant into the injection well is maintained until the fire reaches the bottom of the injection well in the RCL or that of the production well in the FCL. This outcome is accompanied by a significant drop in the injection pressure indicating creation of a low hydraulic resistance link between the wells, which establishes a low hydraulic resistance path between the two wells.

* Corresponding author: Tel.: (61-7)33656073 Fax: (61-7)33653670
E-mail address: d.saulov@uq.edu.au
[1] Ergo Exergy Technologies Inc., 465 Rue St. Jean, Porte 508, Montreal Quebec H2Y 2R6, Canada
[2] School of Engineering, The University of Queensland, St. Lucia, QLD 4172, Australia
13 July 2007

The combustion linking techniques were invented in the USSR at Podmoskovnaya UCG plant in 1941. Since then, the combustion linking technique was extensively applied and studied in the Soviet operations. The results of these studies were summarized by Skafa [1] and Kreinin et al. [2].

RCL was widely used for the well linking in the Soviet UCG plants at Yuzhno-Abinsk (Siberia), Shatskaya and Podmoskovnaya (Moscow Region), Lisichansk (Ukraine), Angren (Uzbekistan), and others. For example, at Podmoskovnaya UCG plant, the total length of underground channels created by RCL reached up to 5 km per year. RCL was also utilized in the US UCG program in the 1970s and 1980s. Most recently, RCL was successfully used in the UCG operations at Chinchilla (Australia) and Majuba (South Africa). At the same time, FCL was not so prevalent as RCL. It has been observed from practical UCG operations that links between the wells made by FCL have a pear-like shape, while those made by RCL are predominantly tube-like channels. As pointed out by Skafa [1], this results in a sufficiently higher consumption of coal per unit of the link in FCL compared with that in RCL. The linking speed is also considerably lower in FCL.

Both the RCL and the FCL involve filtration of air and product gas through porous media (coal). Combustion linking techniques also involve devolatilisation of coal and chemical reactions in the gas phase and between oxygen in the gas and solid carbon. Devolatilisation of coal and chemical reactions that take place in coal combustion are widely described in the literature (see, for example, Ref. [1]).

Processes, which involve filtration of gases through porous media and chemical reactions, are generically referred to as *filtration combustion*. Filtration combustion has been studied extensively in the literature. The forward

Article published in Energy 33(3) (2008) 446–454

filtration combustion has been studied, for example by Schult et al. [3], Aldushin et al. [4, 5] and Lu and Yortsos [6], while such studies as Refs. [7–14] are devoted to the reverse filtration combustion. The one-temperature model, in which the thermal equilibrium between gas and solid phases is assumed, has been used in most of the previous studies. However, Wahle et al. [15] studied both the forward and the reverse filtration combustion in terms of two-temperature model and determined effects of the gas-solid non-equilibrium on various aspects of filtration combustion. Stability of the flame front in the filtration combustion has also been studied extensively (see, for example, Refs. [7, 11, 13, 16, 17]).

In the present study, we use the previously developed techniques to analyse the filtration combustion of coal in the context of UCG. In particular, we investigate FCL using two-dimensional model for a gas flow though a coal seam. Stability of the flame in FCL is also analysed.

2. Basic Relations of Filtration Combustion

In the present study, we, to a large extent, follow the principle formulation of filtration combustion used by Schult et al. [3, 10] and recently by Liu et. al. [12]. Unlike one of Britten and Krantz [7], this formulation provides for analysing both oxygen-deficient and carbon-deficient flames. We assume, however, as did Britten and Krantz [7], that gas phase in the reaction zone is not dominated by diffusion. In the present analysis of the plane flame we use a unified notation for the reverse filtration combustion, as well as the reaction leading and reaction trailing regimes of the forward filtration combustion which are described in detail in the literature (see, for example, [3, 18]). We do not consider the liquid phase separately, assuming that the underground water is either supplied with the injection flow or represents the coal moisture content. Hence only two phases, the gas and the solid, need to be indexed explicitly.

2.1. *The modelling equations*

The equations governing transport and reactions in porous media are represented by the equations of conservation of mass, energy and species and the Darcy low, which can be written in the form

$$\frac{\partial \overline{\rho}}{\partial t} + \nabla\cdot(\overline{\mathbf{m}}) = 0 \; ; \tag{1}$$

$$\frac{\partial \overline{\rho_i}}{\partial t} + \nabla\cdot(\overline{\mathbf{m}_i}) = \overline{W_i} \; ; \tag{2}$$

$$\frac{\partial \overline{\rho h}}{\partial t} + \nabla\cdot(\overline{\mathbf{m}h}) - \nabla\cdot\left(\lambda\nabla(T)\right) = 0 \; ; \tag{3}$$

$$\mathbf{u} = -\frac{\kappa}{\eta}\nabla\cdot p \; . \tag{4}$$

Here, $\mathbf{m}_i \equiv \mathbf{v}_i\rho_i$ is the mass flux of the i^{th} species, ρ_i is its density. In the gas phase, ρ_i is the partial density of the i^{th} species, while in the solid phase, ρ_i is fictitious "partial density" of the i^{th} species, which is the product of the actual density and the volume fraction of the species "i" in the solid phase. The mass fraction of the species $Y_{g(s),i}$ in the gas (solid) phase is determined by $Y_{g(s),i} = \rho_i/\rho_{g(s)}$, where $\rho_{g(s)}$ is the gas (solid) density.

The species velocities $\mathbf{v}_i$ are given in the moving system of coordinates attached to the flame front, which is moved with the velocity $\mathbf{s}$ in a stationary frame of reference. The filtration velocity $\mathbf{u}$ is given in the stationary frame of reference. The velocity of the solid phase $\mathbf{v}_s$ is then expressed by $\mathbf{v}_s = -\mathbf{s}$, while the velocity of the gas phase $\mathbf{v}_g$ is expressed by $\mathbf{v}_g = \mathbf{u} + \mathbf{s}$ in the reverse combustion and by $\mathbf{g}_s = \mathbf{u} - \mathbf{s}$ in the forward combustion. The velocity of the species "i" coincides either with the $\mathbf{v}_g$, if the species belongs to the gas phase, or with the $\mathbf{v}_s$, if the species is solid. W_i is the chemical reaction source terms of the i^{th} species; κ is the permeability of the porous media; η is the dynamic viscosity of the gas; and λ is the heat conductivity coefficient. The total enthalpy of the i^{th} species per unit of mass is denoted by h_i. The over-bar denotes the superficial averages: $\overline{\mathbf{m}} = \sum_i \phi_i\mathbf{m}_i$ and $\overline{\mathbf{m}h} = \sum_i \phi_i\mathbf{m}_i h_i$. The summation is performed over all species (reactants and products) in all phases. If the species "i" is not present at a particular location, its density ρ_i assumed to be zero. The specific volumes ϕ occupied by the phases (gas or solid) are determined by the porosity of the solid phase. It should be noted, that both the velocity $\mathbf{v}$ and the specific volume ϕ are the same for all species of a given phase, although $\mathbf{v}$ and ϕ are, generally, different for different phases. The averages that are applied to a specific phase involve summation only over the species of this phase. The averages that are applied to a single species such as $\overline{\mathbf{m}_i} = \phi_i\mathbf{m}_i$ do not involve summation. The temperature T is considered to be the same for all phases and does not need averaging. The intrinsic averages simply coincide with the values determined within a specific phase, since we do not consider variations of the values in the inter-particle space. Hence, no special notation is needed here for intrinsic averages. The temporal pressure derivative $\partial p/\partial t$ is conventionally neglected in the energy equation.

All of the reactions that take place in the coal combustion are presumed to form a global reaction, which takes the form

$$\mu_g^-(\mathrm{G})^- + \mu_s^-(\mathrm{S})^- \rightarrow \mu_g^+(\mathrm{G})^+ + \mu_s^+(\mathrm{S})^+ \tag{5}$$

or, in terms of species,

$$\sum_i \mu_i^-(\mathrm{Species})_i \rightarrow \sum_i \mu_i^+(\mathrm{Species})_i \; . \tag{6}$$

The coefficients μ_i are on the mass basis. The superscripts "$-$" and "$+$" denote values before and after the reaction respectively and $(\mu_i^+ - \mu_i^-)$ represents the mass change of i^{th} species in the reaction. In the rest of the paper we put $\mu_g^- \equiv 1$ without loss of generality. The global reaction is presumed to be specified so that the stoichiometric coefficients depend on μ_s^- so that $\mu_i^\pm = \mu_i^\pm(\mu_s^-)$ for any species "i" (or phase

"i"). For any i and j, the species source terms $\overline{W_i}$ and $\overline{W_j}$ are related to one another by

$$\frac{\overline{W_i}}{\mu_i^+ - \mu_i^-} = \frac{\overline{W_j}}{\mu_j^+ - \mu_j^-} \ . \tag{7}$$

The total enthalpy h_i of each species can be represented as a sum of the sensible enthalpy and enthalpy of formation $h_i = h_i^{(s)} + h_i^\circ$, where the sensible enthalpy $h_i^{(s)} = h_i^{(s)}(T)$ is a function of temperature and the enthalpy of formation h_i° is defined as the enthalpy at a certain reference temperature T°. The conventional value of T° is 25^0C. In the considered problem, however, the best choice for T°, which accurately defines the heating value of the reaction, would be a constant temperature that is close to the temperature in the reaction zone.

2.2. *The Combustion Temperature in the Plane Flame*

Schult et al. [3] analysed traveling waves in the forward filtration combustion under adiabatic conditions (no heat losses to the environment) using rigorous asymptotic techniques, although assuming that the enthalpy of the reaction is constant. It was demonstrated that two structures, namely, reaction leading and reaction trailing, of traveling waves are possible. Temperature profiles of the traveling waves in different regimes of filtration combustion are schematically presented in Fig. 2, while temperature profiles in the corresponding flames are given in Fig. 3.

For each of these structures there exist stoichiometric (transport-limited) and kinetic (temperature-limited) regimes. Unlike the reverse filtration combustion, the combustion temperature in the forward filtration combustion exceeds the adiabatic temperature. This superadiabatic effect occurs due to the energy accumulation between the flame front and the heat exchange layer, which propagates slower(faster) than the flame in the reaction leading(trailing) wave structure (see, for example, the works by Schult et al. [3] and by Aldushin et al. [5].

Following the approach used by Blinderman and Klimenko [13], we compare the combustion temperatures in the FCL and RCL and discuss the regimes of the FCL. We use the system of coordinates that is attached to the flame with the x-axis normal to the flame front and pointing in the direction of the gas flow. The flame is interpreted as the reaction zone combined with the adjacent layer of rapid variation in temperature (see Fig. 3). Eqs. (1-3) then take the form

$$\frac{\partial \overline{m}}{\partial x} = 0 \tag{8}$$

$$\frac{\partial \overline{m_i}}{\partial x} = \overline{W_i}, \tag{9}$$

$$\frac{\partial \overline{mh}}{\partial x} - \frac{\partial}{\partial x}\left(\lambda \frac{\partial T}{\partial x}\right) = 0 \ . \tag{10}$$

Integration of Eqs. (8)-(10) across the flame yields

$$(\overline{m})_{(+f)} = (\overline{m})_{(-f)}, \tag{11}$$

$$(\overline{m_i})_{(+f)} = (\overline{m_i})_{(-f)} + \int_{(-f)}^{(+f)} \overline{W_i} dx, \tag{12}$$

$$(\overline{mh})_{(+f)} = (\overline{mh})_{(-f)}. \tag{13}$$

Here, the subscript "$-f$" is used to denote values before the flame while the subscript "$+f$" denotes values after the flame front in the direction of the gas flow (see Fig. 3).

To rewrite equation (13) in terms of the stoichiometric coefficients of the reaction $\mu_i^\pm$, we note that the the reaction coefficients are linked to the mass fluxes by the equations

$$\mu_i^- = \left|\frac{(\overline{m_i})^-}{(\overline{m_g})^-}\right|, \quad \mu_i^+ = \left|\frac{(\overline{m_i})^+}{(\overline{m_g})^-}\right|. \tag{14}$$

Here, the superscripts "$-$" and "$+$" denote the values before and after the reaction, respectively. The superscripts should be clearly distinguished from the subscripts "$-f$" and "$+f$", which indicate the location with respect to the flame in the direction of the gas flow. Unlike the RCL, where all the reactants are located before the flame and all the products are located after the flame, in the FCL both reactants and products are present before the flame and after the flame as well. Solids represent products in front of the flame and reactants behind the flame, while gas species represent reactants in front of and products behind the flame. It is also worth noting that mass fluxes of the gas species are positive, while those of solids are negative, since the velocities of gas and solid phases are opposite in the FCL. Dividing Eq. (13) by $(\overline{m_g})^-$, separating gas and solid species and using equations (14) we obtain:

$$\begin{aligned} &\overline{h_g}(T_{(-f)}) - \mu_s^+ \overline{h_s}(T_{(-f)}) \\ &= \mu_g^+ \overline{h_g}(T_{(+f)}) - \mu_s^- \overline{h_s}(T_{(+f)}). \end{aligned} \tag{15}$$

Here, the unknown combustion temperature $T_b = T_{(-f)}$ in the reaction leading wave structure, while $T_b = T_{(+f)}$ in the reaction trailing structure. In the case of reaction leading structure, the $T_{(+f)}$ is the ambient temperature of coal. This temperature is not necessarily the same as the ambient temperature of the injected gas, which is equal to $T_{(-f)}$ in the reaction trailing structure.

In the RCL the enthalpy flow balance equation (13) takes the form

$$\begin{aligned} &\overline{h_g}(T_{(-f)}) + \mu_s^- \overline{h_s}(T_{(-f)}) = \\ &\mu_g^+ \overline{h_g}(T_{(+f)}) + \mu_s^- \overline{h_s}(T_{(+f)}). \end{aligned} \tag{16}$$

Here, $T_b = T_{(+f)}$ and $T_{(-f)}$ is the ambient temperature of the injected gas and solid fuel.

3. The Combustion Regime in FCL

In order to compare the forward and reverse combustion linking, we use the same major reaction and the same fuel parameters as used in the previous work [13]. The solution of Eq. (15) that corresponds to the reaction leading structure does not exists for the selected fuel. Numerical simulation runs demonstrated that the reaction leading solution becomes possible only when the amount of inert solids (ash

and water) in the fuel (coal) exceeds 90 percent by weight. Since coal with such a high inerts content is not usually possible to utilize, we exclude the reaction leading structure from the later consideration.

The the combustion temperatures as functions of the fuel to air ratio in the forward wave with the reaction trailing structure and in the reverse wave are presented in Fig. 4. As discussed, for example, by Schult et al. [3], the reaction can not be fuel deficient in the reaction trailing structure and oxygen deficient in the reaction leading structure, since oxygen and fuel can not coexist at high temperature. For this reason, we exclude from the plot the fuel deficient branch of the combustion temperature curve in the forward wave.

As discussed, for example, by Britten and Krantz [7] and by Blinderman and Klimenko [13], the reaction in the RCL is, generally, temperature-limited . A typical mass flux of the deficient component (oxygen) in RCL and in the gasification process proper is relatively large. The flux is proportional to the filtration velocity $\mathbf{u}$ and exceeds some critical value, below which the reaction becomes transport-limited. The critical value of the flux, in turn, exponentially depends on the combustion temperature.

However, as shown in Fig. 4, the combustion temperature in the forward filtration combustion is significantly higher than that in the reverse combustion. Due to the exponential dependence of the flux critical value on the combustion temperature, the critical value of the flux in the FCL is by several orders of magnitude larger than that in the RCL. At the same time, the filtration velocity in the FCL is of the same order of magnitude as that in RCL.

As a result, in the case of the FCL without heat losses, the flux critical value becomes practically unattainable and we assume hereinafter that all oxygen that has arrived at a coal surface reacts instantaneously. In this case, the flame propagation velocity $\mathbf{s}$ is proportional to the filtration velocity and, unlike in the RCL, is independent of the combustion temperature. Taking into account that for coal $\phi_g\rho_g \ll \phi_s\rho_s$ and μ_s^- is of the order of unity, one can obtain

$$\mathbf{s} = \frac{(\phi_g\rho_g)_{(-f)}}{\hat{\mu}_s^-\,(\phi_s\rho_s)_{(+f)}}\mathbf{u}, \tag{17}$$

where $\hat{\mu}_s^-$ is the stoichiometric fuel to air ratio.

4. Two-dimensional model of FCL

In modelling of the cavity growth in FCL, we assume that the thickness of the coal seam is small compared with the distance between injection and production wells. This implies that the flow of gas in the coal seam is virtually two-dimensional. We also assume that the flow is quasi-stationery. This assumption is based on the fact that flame velocity $\mathbf{s}$ is small compared with the filtration velocity $\mathbf{u}$. We also assume that gas does not escape from the coal seam into surrounding rock.

The filtration of gas through the coal seam is governed by *the Darcy low* (see Eq. (4)), *the continuity equation*

$$\nabla(\rho\mathbf{u}) = 0 \tag{18}$$

and *the equation of state*

$$\rho = \frac{m_0}{RT}p\ . \tag{19}$$

Here, ρ and m_0 are density and molar mass of gas, respectively; pressure and absolute temperature are denoted by p and T; R is the universal gas constant.

Combining Eqs. (4), (18) and (19) one verifies that the pressure distribution in the coal seam is governed by the following Laplace equation

$$-\frac{m_0\kappa}{2RT\mu}\nabla^2 p^2 = 0, \tag{20}$$

subject to the boundary conditions:

$$\begin{aligned} &\text{B.C.1: } p = p_{\rm iw};\ \text{in the injection well,}\\ &\text{B.C.2: } p = p_{\rm pw};\ \text{in the production well.}\end{aligned} \tag{21}$$

where $p_{\rm iw}$ and $p_{\rm pw}$ are the pressure values in injection and production wells, respectively.

4.1. *Linking time under constant pressure difference*

Consider FCL of two wells initially separated by the distance $2L$ and assume that pressure values in the injection well $p_{\rm iw}$ and the production well $p_{\rm pw}$ are maintained constant in the linking process. Initial radii of the wells are assumed to be small compared to the distance between the wells. Select the frame of reference so that the centres of the injection and production wells are on the x-axis with coordinates $-L$ and $+L$, respectively. The linking time t_1 can be calculated as

$$t_1 = \int_{-L}^{+L}\frac{dx}{s_{\rm lp}}\ , \tag{22}$$

where $s_{\rm lp}$ is the velocity of the combustion front at the leading point along x-axis.

Since all coal is consumed in the reaction and air pressure in the injection well is maintained constant, Eq. (17) takes the form

$$\mathbf{s} = \frac{m_0 p_{iw}}{RT\hat{\mu}_s^-\,\rho_{\rm c}}\mathbf{u} \equiv \alpha\mathbf{u}\ , \tag{23}$$

where $\rho_{\rm c}$ is the coal density.

Normalising distances by L and introducing the dimensionless pressure f by

$$f \equiv \left(p^2 - \frac{p_{\rm iw}^2 + p_{\rm pw}^2}{2}\right)\frac{2}{p_{\rm iw}^2 - p_{\rm pw}^2}\ , \tag{24}$$

one finds that

$$t_1 = -\frac{4\eta p_{\rm iw}L^2}{\alpha\kappa\left(p_{\rm iw}^2 - p_{\rm pw}^2\right)}\int_{-1}^{+1}\frac{d\xi}{(\partial f/\partial\xi)_{\rm lp}}\ . \tag{25}$$

Here, $\xi = x/L$ and $(\partial f/\partial\xi)_{\rm lp}$ is dimensionless front propagation velocity at the leading point along the ξ-axes.

Note that f is a solution of the following boundary value problem

$$\begin{aligned} &\nabla^2 f = 0 && \text{subject to:} \\ &\text{B.C.1: } f = 1; && \text{in the injection well,} \\ &\text{B.C.2: } f = -1; && \text{in the production well.} \end{aligned} \tag{26}$$

Note also that

$$t_0 = \int_{-1}^{1} \frac{d\xi}{(\partial f/\partial \xi)_{\text{lp}}} \ . \tag{27}$$

is the "linking time" for the correspondent moving boundary problem, which has been estimated numerically as follows.

The injection and production well are defined by sets of points on their borders and the function f is calculated using finite-difference method over a rectangular finite domain. The domain dimensions are much larger than the distance between the wells. Then, the formation of the link is modelled by shifting the points on the border of the injection well on the vectors ∇f. After that, the function f is recalculated for the new cavity. These iterations are continued until the cavity reaches the production well. To suppress instabilities the calculated gradients were averaged over five nearest points. The reasons for suppressing instabilities are discussed in Section 5 of this paper.

In order to verify the described algorithm, the growth of the cavity in the steady-state "source-sink" field have been modelled. The results of the calculations are presented in Fig. 5 in comparison with the analytically obtained form of the cavity. As shown in Fig. 5, the effect of averaging of gradients and the finiteness of the calculational domain on the form of the cavity is negligible.

After the verification of the algorithm, the cavity growth have been modelled with recalculations of the function f. The obtained form of the cavity is presented in Fig. 6. The calculated value of t_0 is 1.13. The calculated area of the cavity S_0 is 2.79.

4.2. *Linking time under constant air injection rate*

Now assume that the FCL is carried out with the constant air injection rate $\dot{M}$ that is given on the mass basis. In this case, the linking time t_2 can be calculated using S_0 as follows.

$$t_2 = \frac{S_0 b \rho_{\text{c}} L^2}{\dot{M} \hat{\mu}_s^-} \ , \tag{28}$$

where L is the half-distance between the wells, b is the coal seam thickness, ρ_{c} is the coal density, and $\hat{\mu}_s^-$ is the stoichiometric fuel to air ratio.

5. Discussion

Eqs. (25) and (28) represent important results. The equations demonstrate that (in the absence of developing instabilities of the combustion front) linking time is proportional to squared distance between the wells. This implies that connecting the injection and production wells using FCL takes relatively long time and results in consumption of a substantial amount of coal. For example, if air is injected at the rate of 2000 normal cubic meters per hour, the estimated time for linking two wells at the distance of 30 m. in a coal seam of 2 m. thickness will be approximately 228 days. Such a long linking time is not suitable for a viable UCG operation. Furthermore, a prolonged exposure of the local aquifer to the high pressure product gas may result in contamination of the ground water system. The estimated amount of coal consumed in the linking process is approximately 1632 tones.

These results are in qualitative agreement with the experimental observations. As reported by Skafa [1], the cavity formed in FCL has a pear-like shape, while RCL leads to a relatively narrow channel between the injection and production wells. As a result, more air is required and more coal is consumed per unit length of link in the case of FCL. According to Skafa, FCL is also characterised by smaller linking speed (compared to RCL).

Note that heat losses to the surroundings have not been taken into account in the analysis above. Unlike RCL, where combustion temperature is a critical factor affecting the flame propagation, heat losses are less important in the case of FCL. Note that the combustion temperature in the case of FCL is much higher than that in RCL due to the superadiabatic effect. This allows us to assume that all oxygen that has arrived at a coal surface reacts instantaneously. Qualitative agreement of the obtained results with the experimental observations can be considered as an indication that, in practical FCL conditions, heat losses are relatively small to switch the combustion to the transport-limited regime.

Note also that the estimates above are obtained assuming stability of the combustion front. At the same time, inhomogeneity of real coal seams as well as changes in coal permeability due to devolatilisation favours creation and development of fingering instabilities. The role of instabilities in FCL is briefly discussed below. Detailed analysis of instabilities in context of FCL, however, is beyond the scope of the present study.

Development of instabilities of the combustion front in FCL towards the production well can potentially increase the linking speed and reduce the amount of coal consumed in the linking process. There is no reason, however, for the instabilities to develop in the desirable direction towards the production well. Development of the instabilities in the opposite direction (or along any streamline that does not reach the production well in a reasonable time) can result in a significant increase in linking time and the amount of coal consumed in the linking process.

Another factor that can be an obstacle for successful FCL is devolatilisation of coal and subsequent condensation of the coal volatile matter. Coal volatile matter is released in the heat wave associated with the combustion front. As the gas leaves the heat wave and propagates further through

the coal seam, it cools down. Some part of the released volatile matter is condensed and can block coal pores. This results in a decrease in coal permeability in the direction of the developing instability. The permeability decrease, in turn, results in a reduction of the gas flow rate and leads to slower flame propagation in the direction of the developing instability.

These factors indicate that FCL may not be a reliable technique for initial linking of the wells. Forward combustion, however, can be used for widening hydraulic links between the wells which either exist naturally or have been preliminary established using, for example, hydrofracturing. The link widening process is outlined below.

Consider a narrow fracture in a coal seam. Assume that the fracture is open enough so that it is not blocked by condensed volatile matter. At practical air flow rates, the flow in a narrow channel is turbulent, which implies that effective diffusion of oxygen toward the channel wall is high. Since oxygen reaching the fracture wall is completely consumed in the reactions due to the high temperature of the wall, all oxygen in the gas would be consumed in a short distance (several diameters) along the fracture. This result in widening of the initial part of the fracture, while the rest of it would remain practically unchanged. The initial part would continue to widen, until the gas flow in the fracture becomes laminar and effective diffusion of oxygen towards the fracture wall decreases dramatically. This would result in penetration of a substantial part of unreacted oxidant further along the channel and subsequent widening the next section of the channel. The resulting diameter of the widened channel will correspond to transition between turbulent and laminar flows.

Diffusion of oxygen also plays a key role in developing of instabilities in the FCL. Unlike in the RCL, where instabilities of combustion front result in formation of relatively narrow and long channels, the development of narrow instabilities in the FCL seems to be impossible due to insufficient flux of oxidant to the leading points of the instabilities. The authors are conducting further study of this process to refine understanding of the role of instabilities in the FCL and quantify their effect.

6. Conclusions

(i) The theoretical framework and numerical model of FCL are proposed and validated in this study using comparison with previous work by the authors on RCL in UCG. The FCL model appears to provide realistic qualitative results for FCL in coal seams.

(ii) In the specific UCG conditions used for comparison of RCL and FCL, the speed and efficiency of linking are considerably lower in case of the FCL.

(iii) Further studies that are being conducted by the authors including numerical experiments on FCL in various conditions representing realistic parameters of UCG operations assist in optimization of FCL and in determining specific UCG conditions when FCL is applicable and effective.

(iv) The approach to FCL described in the paper is being applied to the problem of enlargement of natural and artificial fractures in the coal seam in the process of UCG.

Acknowledgement

The work that has been conducted in the University of Queensland was supported by the Australian Research Council and Linc Energy Ltd.

References

[1] Skafa PV. Underground Coal Gasification. Gosgortechizdat, 1960 (in Russian)

[2] Kreinin EV, Fedorov NA, Zvyagintsev KN, Pyankova TM. Underground Gasification of Coal Seams. Moscow: Nedra, 1982 (in Russian)

[3] Schult DA, Matkowsky BJ, Volpert VA, Fernandez-Pello AC. Forced forward smolder combustion. Combustion and Flame 1996; 104: 1-26

[4] Aldushin AP, Matkowsky BJ, Schult DA. Upward buoyant filtration combustion. Journal of Engineering Mathematics 1997; 31: 205234

[5] Aldushin AP, Rumanov IE, Matkowsky BJ. Maximal energy accumulation in a superadiabatic filtration combustion wave. Combustion and Flame 1999; 118: 76-90

[6] Lu C, Yortsos YC.Dynamics of forward filtration combustion at the pore-network level. AIChE Journal 2005; 51: 1279-1296

[7] Britten JA, Krantz WB. Linear stability of planar reverse combustion in porous media. Combustion and Flame 1985; 60: 125-140

[8] Ohlemiller TJ. Modeling of smoldering combustion propagation. Progress in Energy and Combustion Science 1985; 11: 277-310

[9] Britten JA, Krantz WB. Asymptotic analysis of planar nonadiabatic reverse combustion fronts in porous media. Combustion and Flame 1986; 101: 151-161

[10] Schult DA, Matkowsky BJ, Volpert VA, Fernandez-Pello AC. Propagation and extinction of forced opposed flow smolder waves. Combustion and Flame 1995; 101: 471-460

[11] Schult DA. Bayliss A, Matkowsky BJ. Traveling waves in natural counterflow filtration combustion and their stability. SIAM Journal on Applied Mathematics 1998; 58(3): 806-856

[12] Liu Y, Chen M, Buckmaster J, Jackson T. Smolder waves, smolder spots, and the genesis of tribrachial structures in smolder combustion. Proceedings of the Combustion Institute 2005; 30: 323-329

[13] Blinderman MS, Klimenko AY. Theory of reverse combustion linking, Combustion and Flame, accepted for publication.
[14] Lu C, Yortsos YC. Pattern formation in reverse filtration combustion. Physical Review E 2005; 72: 036201
[15] Wahle C W, Matkowsky BJ, Aldushin AP. Effects of gas-solid nonequilibrium in filtration combustion. Combustion Science and Technology 2003; 175: 1389-1499
[16] Aldushin AP, Kasparyan SG. Stability of stationary filtration combustion waves. Combustion, Explosion, and Shock Waves 1981; 17(6): 37-49
[17] Kakutkina NA. Some stability aspects of gas combustion in porous media. Combustion, Explosion, and Shock Waves 2005; 41(4): 395-404
[18] Akkutlu IY, Yortsos YC. The dynamics of in-situ combustion fronts in porous media. Combustion and Flame 2003; 134(3): 229-247

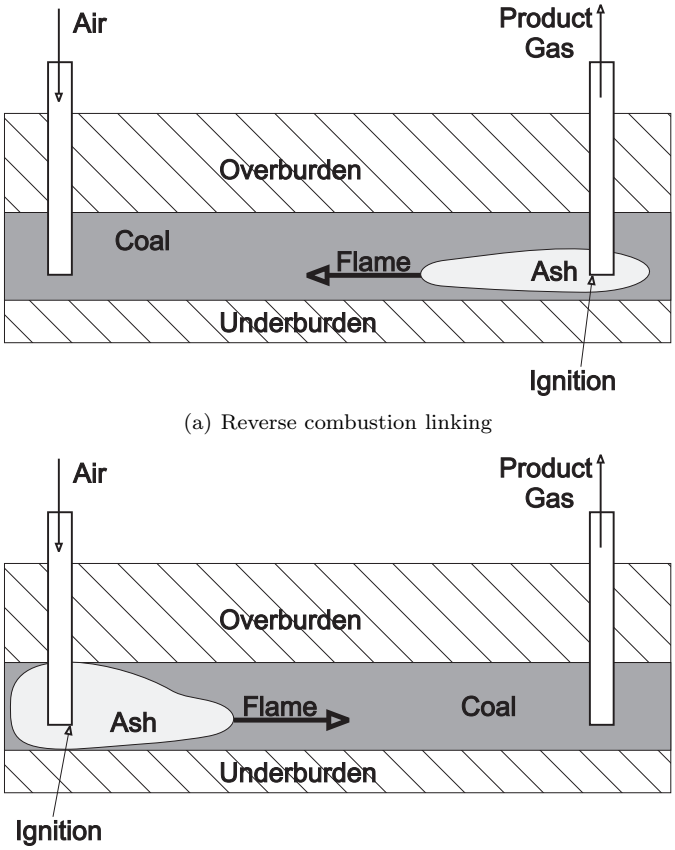

(a) Reverse combustion linking

(b) Forward combustion linking

Fig. 1. Schematic views of the reverse and forward combustion linking in UCG

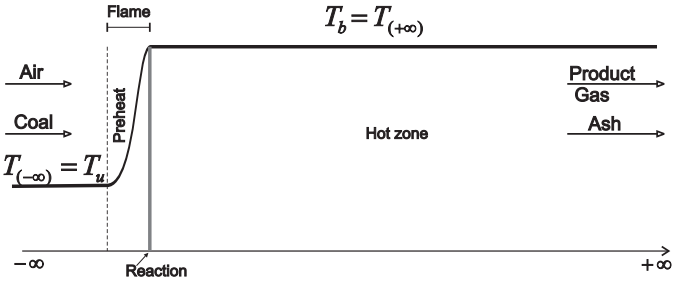

(a) reverse filtration combustion

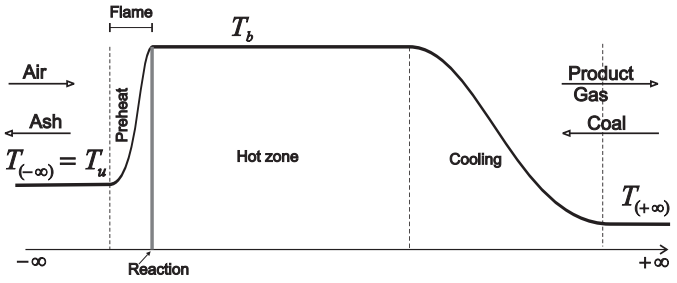

(b) forward filtration combustion with the reaction trailing structure

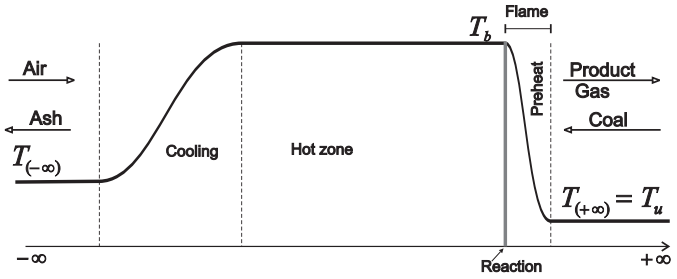

(c) forward filtration combustion with the reaction leading structure

Fig. 2. Temperature profiles of the traveling waves in different regimes of filtration combustion

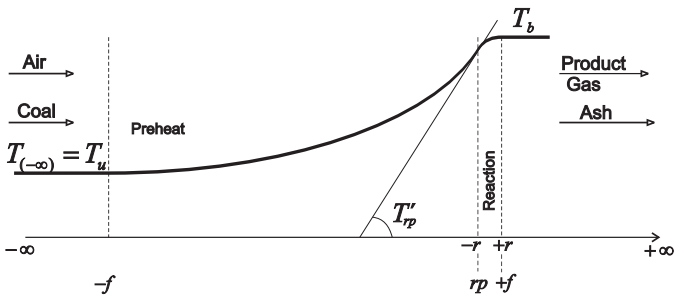

(a) reverse filtration combustion

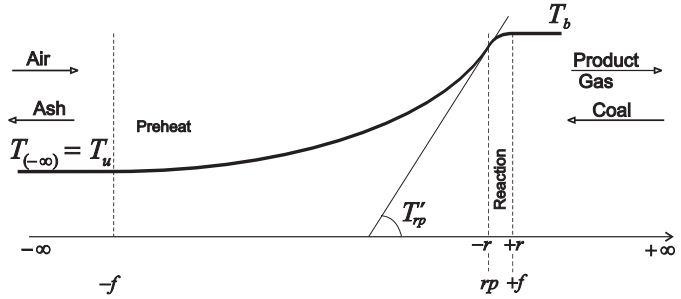

(b) forward filtration combustion with the reaction trailing structure

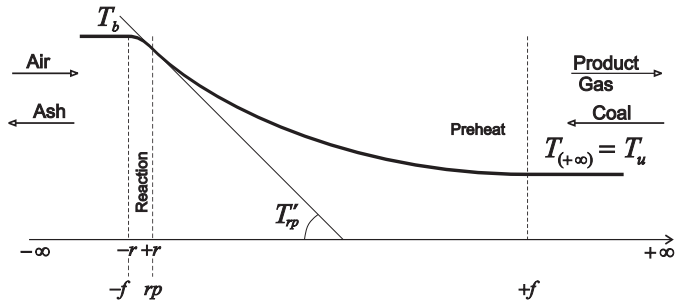

(c) forward filtration combustion with the reaction leading structure

Fig. 3. Temperature profiles of the flames in different regimes of filtration combustion

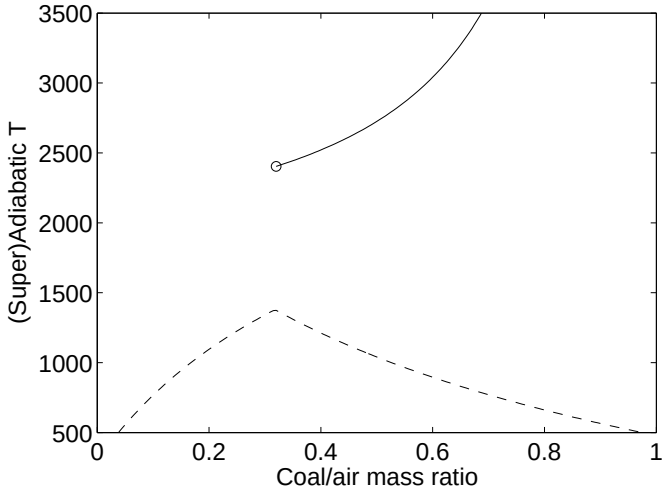

Fig. 4. Combustion temperatures in the forward (solid line) and reverse (dashed line) filtration combustion of coal

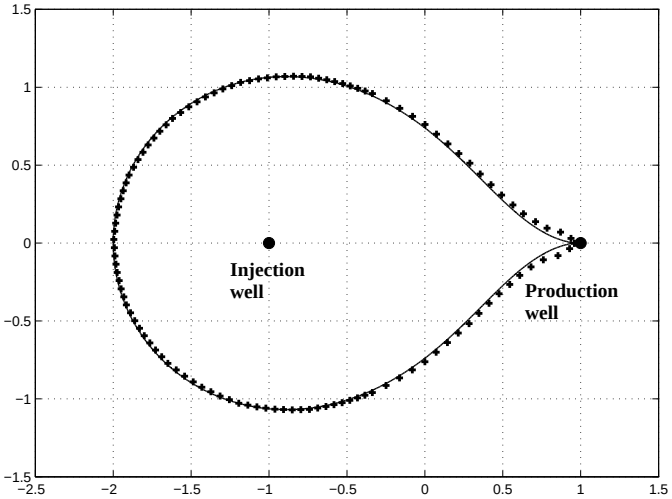

Fig. 5. Shape of the cavity in the constant "source-sink" field. Solid line - analytical curve, Crosses - numerical calculations.

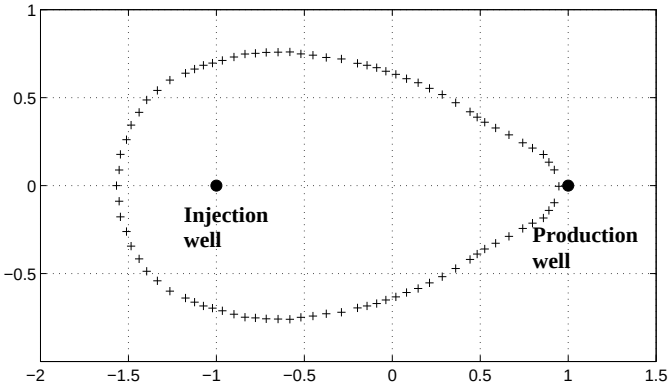

Fig. 6. Shape of the cavity formed in FCL.